Accepted for publication on 7/27/2023 in: *ACS Environmental Science and Technology, Water*
doi: 10.1021/acsestwater.3c00065

Electrolytic Coagulant Generation for Treating Flowback and Produced Water for Reuse

Tenzin Phakdon[a], Jiale Xu[b], James Farrell[a*]

[a]Department of Chemical and Environmental Engineering

University of Arizona, Tucson AZ 85721

[b]Civil, Construction and Environmental Engineering

North Dakota State University, Fargo, ND 58105

*corresponding author: Department of Chemical and Environmental Engineering, University of Arizona, Tucson, AZ 85721; phone: (1) 520-940-0487; orcid.org/0000-0002-4342-7587; email: farrellj@arizona.edu

Abstract

This research investigated a novel electrochemical process for producing a ferric iron coagulant for use in treating flowback and produced water (FPW) from hydraulic fracturing and oil production operations. The electrolytic coagulant generation (ECG) system uses an electrochemical cell to produce acid and base from oilfield brine solutions. The acid is used to dissolve scrap iron to provide a Fe^{3+} coagulating agent, and the base is used to neutralize the treated water. The costs for generating the ferric iron coagulant were determined as a function of current density and feed water salinity. The process was shown to be effective for removing colloidal bentonite particles from brine solutions. The process has several advantages over conventional electrocoagulation using iron anodes, including: the ability to treat anoxic waters, elimination of electrode fouling, lower cost for the coagulant, and the ability to deliver Fe^{3+} doses greater than 1 mM, since it is not limited by the amount of dissolved oxygen required to oxidize ferrous to ferric iron.

Synopsis

An electrochemical process was used to generate a low-cost ferric iron coagulating agent for treating flowback and produced water for reuse.

Keywords

produced water treatment, coagulation, electrolytic, ferric iron coagulant, electrocoagulation, water electrolysis

Introduction

The use of hydraulic fracturing for recovering oil and gas from low permeability formations requires large quantities of water. In the Permian basin of the southwestern United States, 5 to 12 acre-ft of water are needed to complete each hydraulic fracture (1). In many cases, areas with high levels of unconventional oil and gas production are in water-stressed regions (2). This results in high costs for obtaining and transporting the water needed for hydraulic fracturing operations. Also problematic is that a large fraction of the injected water is recovered as flowback over the early stages of oil and gas production. Flowback and produced water (FPW) recovered along with oil or gas are contaminated with dissolved hydrocarbons, emulsified oil, and suspended and dissolved solids, and must be treated before disposal or reuse.

Treatment options for most FPW are limited by its high salt content, which is generally greater than that of seawater (35,000 mg/L) and is often greater than 200,000 mg/L (3). The most practical and commonly used options for disposal of FPW are deep well injection or reuse in hydraulic fracturing or secondary oil recovery (4,5,6). Treatment of FPW for these uses requires removal of: 1) solids; 2) H_2S; 3) dispersed oil; 4) Fe^{2+}, and sometimes partial removal of other scale forming cations (*e.g.*, Ba^{2+}, Sr^{2+}, Ca^{2+}). Disinfection prior to storage is also desirable to reduce the need for organic disinfectants (*e.g.*, glutaraldehyde) during reuse.

A recent publication reviewed 16 commercialized FPW treatment technologies and 15 of these used electrocoagulation (EC) (7,8,9,10,11). EC targets particulate and emulsified oil removal so that the water can be reused in hydraulic fracturing and secondary oil recovery. Other FPW treatment technologies include biological processes

focused on dissolved hydrocarbon removal (12), and membrane methods that remove particulate, salts, and hydrocarbons (13).

Electrolytic Coagulant Production

Electrocoagulation adds Fe^{2+} or Al^{3+} coagulants into solution via anodic dissolution of metal sheets or plates. The ECG process adds Fe^{3+} to the solution and solves several problems with EC and is illustrated in Figure 1. An electrochemical cell is used to produce acid (H^+) and base (OH^-) via electrolysis of water:

$$anode\ reaction \quad 2\,H_2O \rightarrow O_2 + 4\,H^+ + 4\,e^- \tag{1}$$

$$cathode\ reaction \quad 4\,H_2O + 4\,e^- \rightarrow 2\,H_2 + 4\,OH^- \tag{2}$$

The acid is used to dissolve steel scrap in the form of machine shop turnings or filings to produce the Fe^{2+} necessary to form the coagulant:

$$iron\ dissolution\ reaction \quad 2\,H^+ + Fe \rightarrow Fe^{2+} + H_2 \tag{3}$$

Dissolved O_2 generated by reaction 1 oxidizes Fe^{2+} to Fe^{3+}. The cathode reaction raises the pH of the catholyte solution, which is later used to neutralize the treated water back to its original pH value. In addition to water oxidation, oxidation of Cl^- may also occur and produce $Cl_{2(aq)}$:

$$2\,Cl^-_{(aq)} \rightarrow Cl_{2(aq)} + 2\,e^- \tag{4}$$

The dissolved chlorine rapidly reacts with water to produce hypochlorous (HOCl) and hydrochloric (HCl) acids:

$$Cl_{2(aq)} + H_2O_{(l)} \rightarrow HOCl_{(aq)} + H^+{}_{(aq)} + Cl^-_{(aq)} \tag{5}$$

A small fraction of the anolyte solution that bypasses the scrap iron canister can be used to provide a disinfectant during water storage.

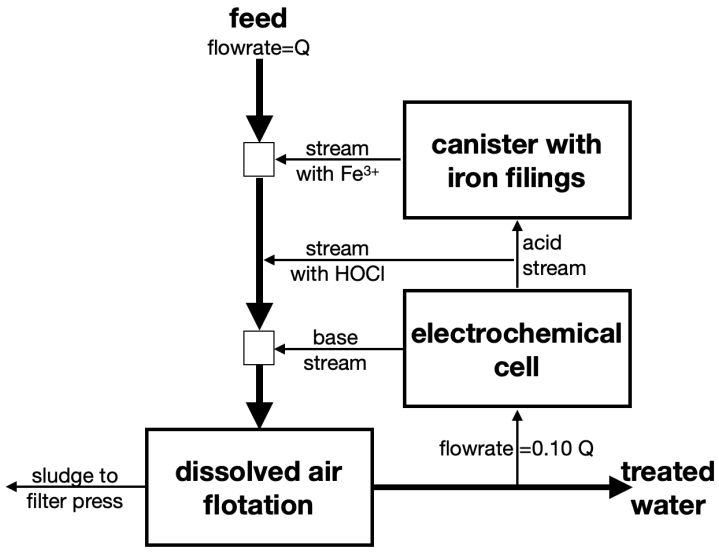

Figure 1. Diagram of the electrolytic coagulant generation system. A fraction of the acid stream bypasses the scrap iron to provide a HOCl disinfectant in the treated water

The ECG process has advantages over both chemical coagulation and EC. Advantages over chemical coagulation are: 1) no net acid is produced since the H^+ formed during ferric hydroxide precipitation is neutralized by OH^- produced at the cathode; 2) coagulant is added more uniformly to the water thereby requiring lower coagulant doses; 3) smaller sludge volume resulting from lower coagulant doses; and 4) lower total cost for the ferric iron coagulant. Advantages of ECG over conventional EC are: 1) significantly lower cost for the iron coagulant; 2) elimination of cathode fouling by mineral scale; 3) elimination of anode fouling at high current densities due to precipitation of coagulant species on anode surface (14); 4) elimination of incomplete iron coagulant usage at high doses (15). In conventional EC, coagulant doses greater than 1 mM lead to magnetite precipitation due to insufficient dissolved oxygen to completely oxidize the Fe^{2+} to Fe^{3+}. The dense particles of magnetite formed under these conditions are not effective for coagulation. This is especially problematic at the high dosages needed for treating FPW,

which have been reported to range from 2.09 (16) to 6.5 mM (17) for iron EC, and 1.83 to 11 mM (18,19) for aluminum EC. A final advantage of the ECG process is its smaller footprint, since the electrochemical cell can operate at current densities more than an order of magnitude greater than those for conventional EC, where the maximum current density is limited to ~10 mA/cm^2 (15). Higher current densities result in oxygen evolution and precipitation of ferric hydroxide and magnetite on the iron anode surface (15).

The goal of this research was to investigate the technical and economic feasibility for replacing conventional EC with electrolytically generated ferric iron. Towards that end, experiments were performed to determine the costs for acid and base production as a function of current density and brine salt concentration. The stoichiometry and kinetics for dissolution of scrap iron were determined and potential electrode fouling issues were investigated.

Materials and Methods

Electrolysis experiments

Electrolysis experiments were performed to determine the energy costs for producing acid and base, and to investigate the formation of hypochlorous acid resulting from oxidation of chloride ions. These experiments employed an ElectroSyn Cell® from Electrocell North America using 2 to 24-unit cells. Both the anode and cathode were platinized titanium with a 2.5 μm-Pt coating and an electroactive area of 400 cm^2 per side. The electrodes were arranged in a monopolar configuration with a 5 mm interelectrode gap. Both sides of each electrode were active, yielding a total anode area of 0.96 m^2 and a total cathode area of 1.0 m^2, as illustrated in Figure S1 in the Supporting Information. Nafion® N-424 cation exchange membranes were used as dividers between the anolyte

and catholyte solutions. A Hydroflow® model S38 electronic water conditioner attached to the catholyte feed pipe was used to reduce mineral scale formation on the cathodes and ion exchange membranes.

Experiments were conducted in a single pass using Na_2SO_4, NaCl and simulated oilfield brine solutions. The experiments were run galvanostatically using current densities ranging from 6.25 to 100 mA/cm^2. Flow rates ranged from 0.125 to 1 L/min per unit cell, yielding mean hydraulic detention times ranging from 0.2 to 1.6 min. Influent and effluent pH values were measured using an Accumet AE10 pH-meter. The concentrations of H^+ and OH^- in the effluent solutions were determined via titration using standardized NaOH and HCl solutions. The applied voltage was recorded over the course of the experiments. Chlorine concentrations in the solutions were measured using the total chlorine DPD method (20). The Faradaic efficiency (ξ) was determined by:

$$\xi = \frac{C\,Q}{I/_F} \times 100\% \tag{6}$$

where C (M) is the concentration of acid or base, Q (L/s) is the volumetric flow rate, I (A) is the applied current and F is the Faraday constant. The energy to generate 1 kmol of acid or base was calculated from:

$$E = \frac{I\,\bar{U}}{2\,C\,Q} \tag{7}$$

where $E\left(\frac{kWh}{kmol}\right)$ is the energy and $\bar{U}(V)$ is the average voltage over the course of each experiment. Because acid and base are produced at the same time and in equal quantities, the total energy required to operate the cell in each experiment was divided by a factor of two to determine separate energy requirements for generation of 1 kmol of acid or 1 kmol of base.

Iron Dissolution Experiments

Experiments were performed to investigate the stoichiometry and kinetics of iron dissolution by the electrochemically produced acid and oxygen. These experiments used Connelly-GPM (Chicago, IL) CC-1004, -8 to +50 mesh metallic iron filings contained in a 30 L PVC tank. Empty bed contact times (EBCT) between the acid solutions and the filings ranged from 1.8 to 14 minutes. Iron concentrations in the effluent stream were determined using a spectrophotometer via the 1,10 phenanthroline method (21).

Suspended Solids Removal

The effect of the electrochemically generated coagulant for lowering turbidity via coagulation/flocculation of suspended solids was investigated using bentonite clay in a simulated oilfield brine solution whose composition is listed in Table 1. Suspensions containing 500 to 1500 mg/L of bentonite were treated with electrochemically generated ferric iron doses ranging from 1.25 to 2.5 mM. Final turbidity and pH values were measured after 2 hours of settling in 1 L Erlenmeyer flasks.

Table 1. Composition of simulated brine solution compared to an oilfield brine from Jal, New Mexico, USA (22).

Parameter	**Jal Well**	**Experiment**
pH	7.3	7.6
Ca^{2+}	4247 mg/L	4240 mg/L
Mg^{2+}	727 mg/L	730 mg/L
HCO_3^-	2867 mg/L	3050 mg/L
Na^+	42,720 mg/L	36,800 mg/L
Cl^-	65,800 mg/L	56,800 mg/L

Results and Discussion

Electrolysis Experiments

Electrochemical production of reagents is often performed in recirculation mode using short hydraulic detention times to minimize mass transfer limitations on reactant conversion. However, for operational simplicity it is desirable to produce high acid and base concentrations in a single pass through the electrochemical cell. This requires high Faradaic efficiencies at low flow rates. Experiments were performed to determine the effect of flow rate on the Faradaic efficiency and concentrations of acid and base that could be produced in a single pass. These experiments were run at a fixed current density of 25 mA/cm^2 using 0.5 M NaCl as the feed solution. At this current density, there were negligible O_2 and H_2 gas bubbles that could decrease the electrical conductivity of the solution and thereby affect the operating voltage.

Figure 2a shows the total acid concentrations, which are the sum of the hydronium ion (H_3O) and the hypochlorous acid (HOCl) concentrations. Increasing the flow rate had a less than proportional decrease in the total acid concentration, yielding increased Faradic efficiencies with increasing flow rate. This can be attributed to greater H^+ diffusion across the Nafion® membrane at lower flow rates due to greater acid concentrations and increased hydraulic detention times in the anode chamber of the electrochemical cell. Figure 2b shows that the Faradaic efficiency reached 96% at a flow rate of 0.5 L/min, which indicates that flow rates in excess of 0.5 L/min per unit cell are not needed to achieve high efficiencies. As shown in Figure 2c, the ratio of HOCl to the total amount of acid produced ranged from 35 to 40% and was only marginally affected by the flow rate. Considering that more than half the H^+ ions passed through the Nafion® membrane at the

lowest flow rate, the near constant ratio of HOCl to total acid indicates that chloride oxidation accounted for a smaller fraction of the total current at lower flow rates. This is consistent with slower rates of Cl^- mass transfer to the electrode surface at lower flow rates, as predicted by boundary layer theory (23). Figure 2d shows the energy requirements per kmol of acid and base produced as a function of flow rate. The decreasing energy costs with increasing flow rate are the result of higher Faradaic efficiencies with increasing flow rate.

Electrolysis experiments were also performed to determine the effect of current density and feed solution composition on the energy costs for producing acid and base. Figure 3 shows the energy costs for producing 1 kmol of acid and 1 kmol of base from Na_2SO_4 and NaCl electrolyte solutions. Persulfate concentrations in the effluent solutions were below the detection limit which indicated no appreciable sulfate oxidation in these experiments. For all feed solutions, the energy requirements increased in a near linear manner with current density. This is expected since the rate of acid production is proportional to the current density but ohmic power dissipation is proportional to the second power of the current density (15). For feed solutions containing only Na_2SO_4, the energy costs decreased with increasing salt concentrations. This can be attributed to increasing solution electrical conductivity with increasing salt concentration. The lowest salt concentration investigated was 35 mM Na_2SO_4, which is equivalent to 5000 mg/L total dissolved solids (TDS). This is at the low end of TDS concentrations in real flowback and produced water (3). The highest salt concentration of 704 mM Na_2SO_4 is equivalent to a TDS concentration of 100,000 mg/L, which is in the mid-range of TDS values found in FPW, which often exceed 250,000 mg/L TDS (3). The two NaCl containing solutions,

which had ionic strength values of 299 and 334 mM, had similar energy costs as the 176 mM Na_2SO_4 solution, which had an ionic strength of 528 mM. This indicates that oxidation of Cl^- was more energetically favorable than water oxidation under these operating conditions.

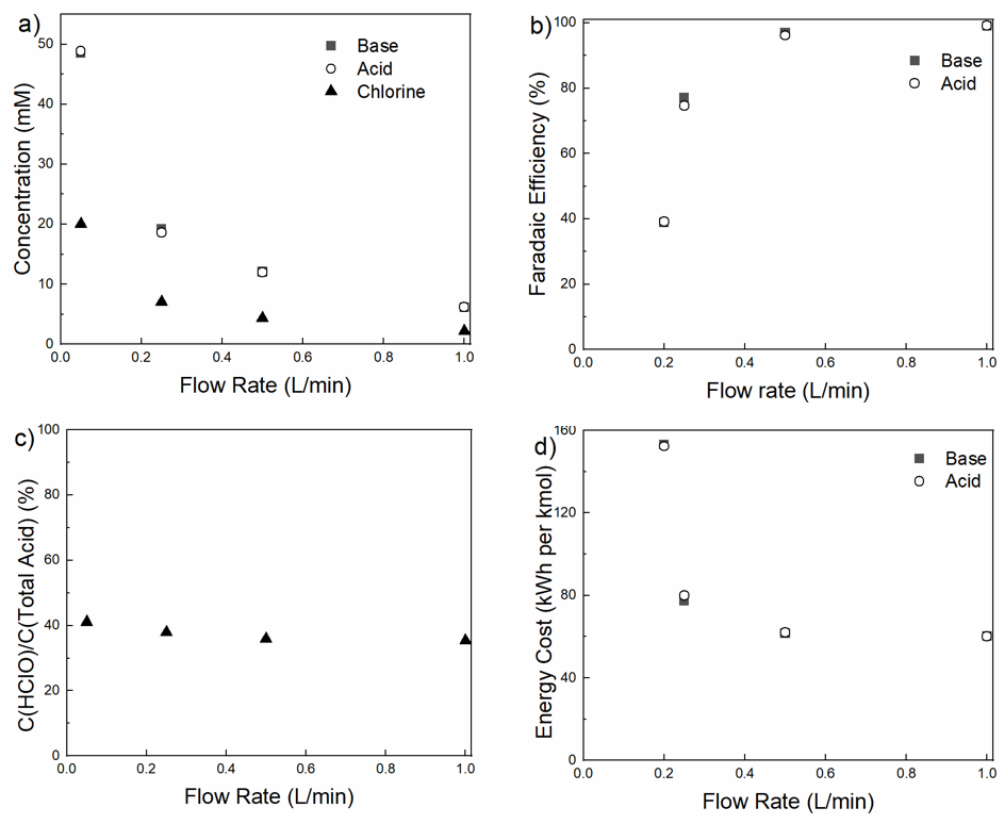

Figure 2. a) Acid, base and HOCl concentrations as a function of flow rate per unit cell; b) Faradaic efficiency for acid and base production; c) fraction of acid present as HOCl; d) Energy requirements per kmol of acid or base as calculated by equation 7.

The energy costs for electrolytic acid and base production are considerably less than costs for purchasing technical grade (*i.e.*, lowest grade) acid and base in multiple ton quantities. Based on the highest energy cost in Figure 3 of 150 kWh per kmol and a US average industrial electricity cost of $0.083 (24), the cost for producing 1 kmol of acid plus

1 kmol of base is $24.90. Approximate costs for technical grade acid and base are $135/kmol for H_2SO_4 (25) and $140 /kmol for NaOH (26). Thus, the electrical energy cost was less than 10% of the cost for purchasing technical grade chemicals.

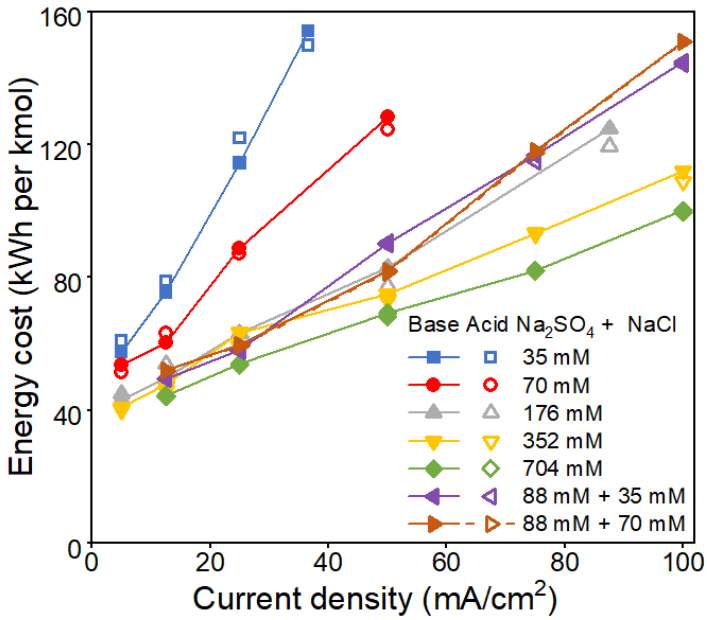

Figure 3. Energy costs per kmol of acid or base produced for different electrolyte solutions.

Iron Dissolution Experiments

Experiments were conducted to determine the stoichiometry between acid consumption and ferric iron generation. Figure 4 shows the moles of acid consumed per mole of iron dissolved. For dissolution of metallic iron by acid, two moles of H^+ are required per mol of Fe^{2+}, as illustrated by equation 3. In addition, one mol of acid is required to oxidize one mole of Fe^{2+}:

$$2Fe^{2+} + 2H^+ + 0.5\ O_{2(aq)} \rightarrow 2Fe^{3+} + H_2O \qquad (8)$$

Thus, three moles of acid should be consumed per mole of Fe^{3+}. However, the data in Figure 4 shows that each mole of Fe^{3+} produced required only 1.6 moles of acid. This can be explained by the fact that O_2 dissolved in the acid can also oxidize metallic iron according to:

$$4Fe_{(s)} + 3O_{2(aq)} + 2H_2O \leftrightarrow 2\,Fe_2O_3 \cdot H_2O_{(s)} \quad (9)$$

Dissolved oxygen may also oxidize Fe^{2+} with concomitant generation of acid, according to: (27,28):

$$4\,Fe^{2+} + O_{2(aq)} + 6H_2O \leftrightarrow 4\,FeOOH_{(s)} + 8\,H^+ \quad (10)$$

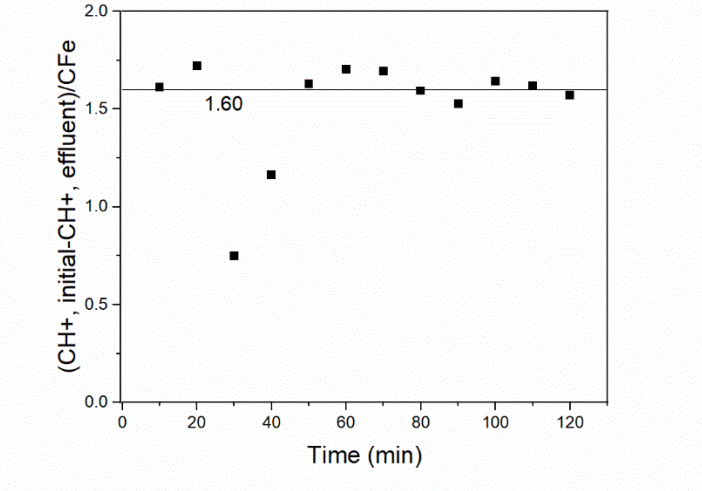

Figure 4. Equivalents of acid consumed per aqueous phase Fe versus elapsed time of operation by electrochemically generated acid.

The technical feasibility for electrochemical coagulant generation requires that the reaction between the acid and the iron filings be sufficiently fast so that only a short contact time is needed. Figure 5 shows the fraction of the acid consumed as a function of the EBCT. In 88 mM sodium sulfate solutions, the fraction of the acid consumed

increased from 36% to 96% by increasing the EBCT from 1.8 to 14 minutes. However, in solutions containing 88 mM Na_2SO_4 plus 35 mM NaCl, >99% of the acid reacted with an EBCT of 2 minutes or less. The faster dissolution results from Cl^- ions preventing formation of a ferric hydroxide passivating layer on the iron (29). Thus, since most FPW contains more than 35 mM of Cl^- ions, a short EBCT can be used to dissolve the iron filings.

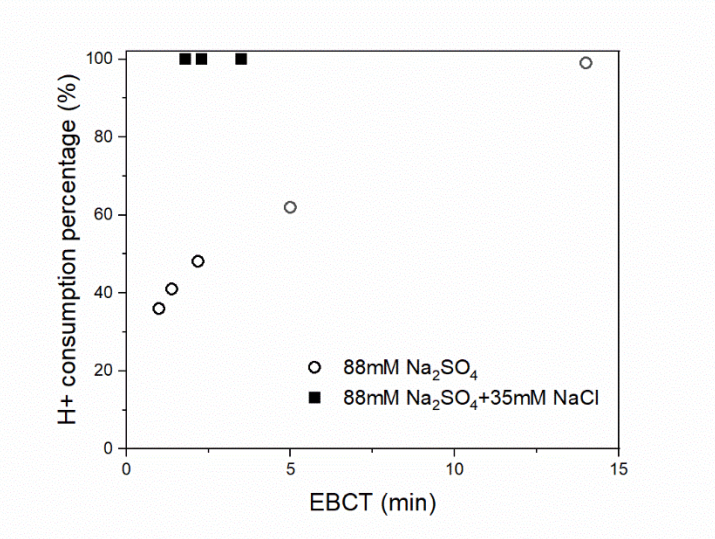

Figure 5. Fractional acid consumption as a function of empty bed contact time (EBCT) in iron filings tank.

Electrode and Membrane Fouling

FPW often contains high concentrations of Ca^{2+} and Mg^{2+} ions that can form $CaCO_3$ or $Mg(OH)_2$ mineral scale at the high pH values in the cathode compartment of the electrochemical cell. Precipitation of $CaCO_3$ or $Mg(OH)_2$ in solution is not problematic since those precipitates will exit the cell in the catholyte stream. However, precipitation of mineral solids on the electrode surface will block electroactive sites and make areas of the electrode surface inactive. In addition, precipitation of mineral solids on the

membrane dividing the electrochemical cell will impede ion transport through the membrane in areas covered with precipitate. If precipitated mineral solids build up on the electrode or membrane, increasing voltages will be needed to maintain the same current. Precipitates on the electrode and membrane can be removed by reversing the polarity of the electrochemical cell. By reversing polarity, the electrode previously serving as the cathode is converted to an anode that produces O_2 and H^+ via water oxidation. The H^+ ions can dissolve precipitated mineral scale on both the membrane and electrode surface.

To investigate electrode and membrane fouling, experiments were performed with feed solutions containing high concentrations of Ca^{2+}, Mg^{2+} and HCO_3^-. The concentrations chosen were selected to approximate produced water from an oil production well in the Permian Basin, as shown in Table 1 (22). Figure 6 shows the applied voltage as a function of time when the cell was operated at a current density of 100 mA/cm^2 in both forward and reverse polarity. Forward polarity corresponds to the operating condition of the treatment system and reverse polarity corresponds to the cleaning cycle. Figure 6 shows the system operating in forward polarity for seven hours. During that time, the cell voltage increased from 6.9 V to 7.1 V. This small change in voltage indicates that fouling by mineral scale does not appear to be a problem. When the polarity was reversed after 7 hours of operation, the voltage increased to 7.6 V but remained relatively stable thereafter. The small increase in voltage in reverse polarity can be attributed to a coating on one side of the Nafion® N-24 membrane that reduces proton diffusion through the membrane. This coating should be facing the anode, and results in greater ohmic voltage loss across the membrane when operated facing the cathode.

At other current densities and for up to 15.5 hours of continuous operation, no significant increases in voltage or cell pressure were observed, as shown in Figure S2 in the Supporting Information. These data show that there was only a small effect of operating time on cell voltage and suggests that there was minimal electrode and membrane fouling. To confirm this, the electrochemical cell was taken apart after operating for two hours in forward polarity at 100 mA/cm^2. Figure S3 in the supporting information shows pictures of the cathode and cathode facing membrane from one of the unit cells. There were no visible precipitates on either the membrane or the electrode. This confirms that electrode and membrane fouling was not a problem under the conditions of these experiments.

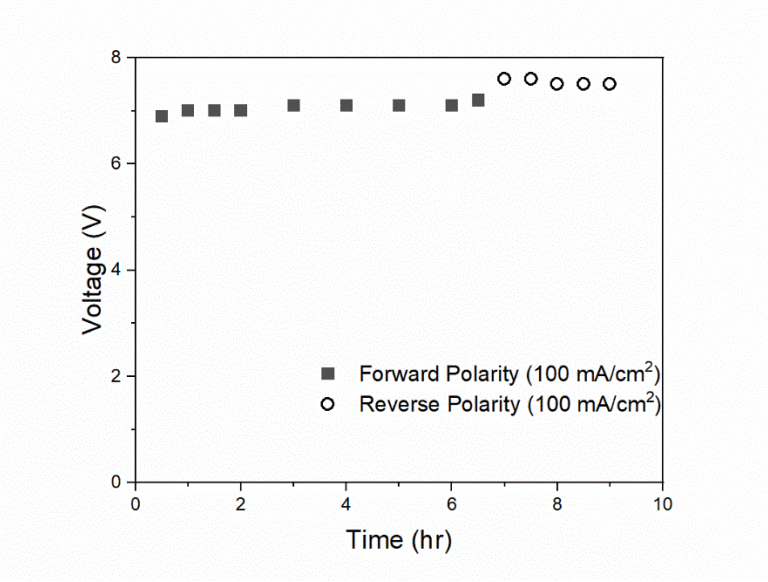

Figure 6. Voltage versus time of operation for forward and reverse polarity at 100 mA/cm^2 using feed water with ion concentrations given in Table 1.

Suspended Solids Removal

Experiments were performed to investigate the effectiveness of the coagulant produced by the ECG process for removing suspended solids. Figure 7 shows initial and

final turbidity and pH values, and final dissolved iron concentrations for a suspension with 1500 mg/L of bentonite clay at an initial pH value of 6.5. Treatment with 1.25 to 2.5 mM ferric iron reduced the turbidity values from 93 NTU to a range of 1.3 to 2.1. These values are lower than the recommended values of <10 NTU for use in hydraulic fracturing (4). Final pH values ranged from 6 to 4.5 and decreased with increasing Fe^{3+} dosage. A possible explanation for the decreases in pH may be a greater contribution of reaction 10 to Fe^{2+} oxidation as compared to reaction 8. Final dissolved iron concentrations ranged from 10 to 13 μM (0.5 – 0.73 mg/L). These values are well below the <10 mg/L guideline for reuse of produced water in hydraulic fracturing (5).

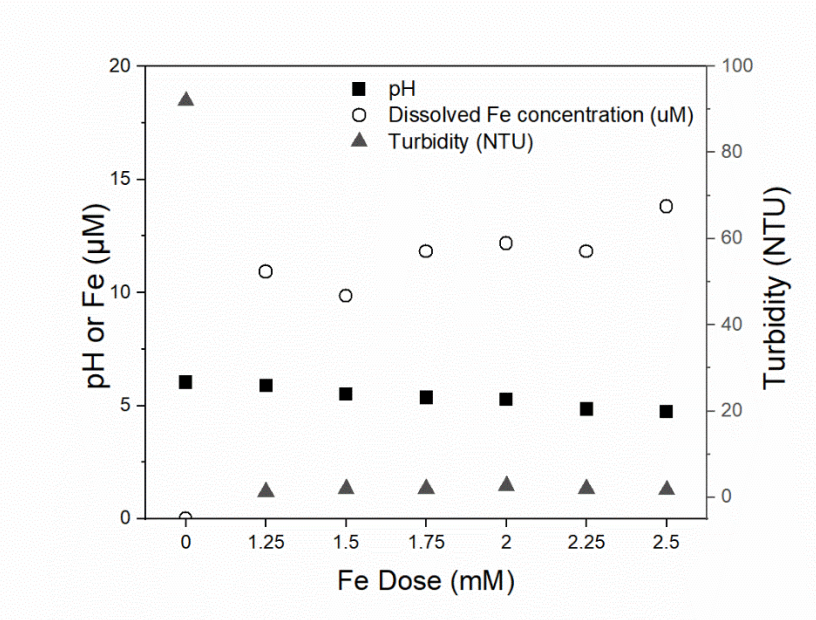

Figure 7. Initial and final pH, turbidity, and dissolved iron concentrations (μM) as a function of iron coagulant dose. Composition of the feed water is given in Table 1. Initial suspended solids concentration was 1500 m/L of bentonite clay with a turbidity of 93 NTU.

Economic Analysis

Figure 8 shows the energy (kWh) required to treat 1 m^3 of water with 1 mM Fe^{3+} coagulant for different feed solutions for the ECG process. The energy costs vary by a

factor of four depending on the current density and feed water salinity. Current costs for scrap iron shavings are approximately $0.35 per lb. The electrical and iron costs can be added to obtain the operating costs for delivering 1 mM Fe^{3+} coagulant per cubic meter of water, as shown in Table 2. The costs in Table 2 were based on the highest energy requirement in Figure 8 of $0.48\ \frac{kWh}{mM-m^3}$ and the U.S. average industrial electricity cost of $0.083 per kWh (24). Including the expense for loss of Pt from the electrodes has a negligible impact on the costs in Table 2. The cell used in this investigation operating at 100 mA/cm^2 passes 1000 A-yr of charge for delivering 2 mM Fe^{3+} into 100,000 m^3 of water. Previous studies have reported a Pt loss of 8 mg/A-yr when operating at 0.1 A/cm^2 in 0.1 M NaCl (30). This corresponds to 8 g of Pt loss per year, which is equivalent to 8 x 10^{-5} g/m^3 of water treated.

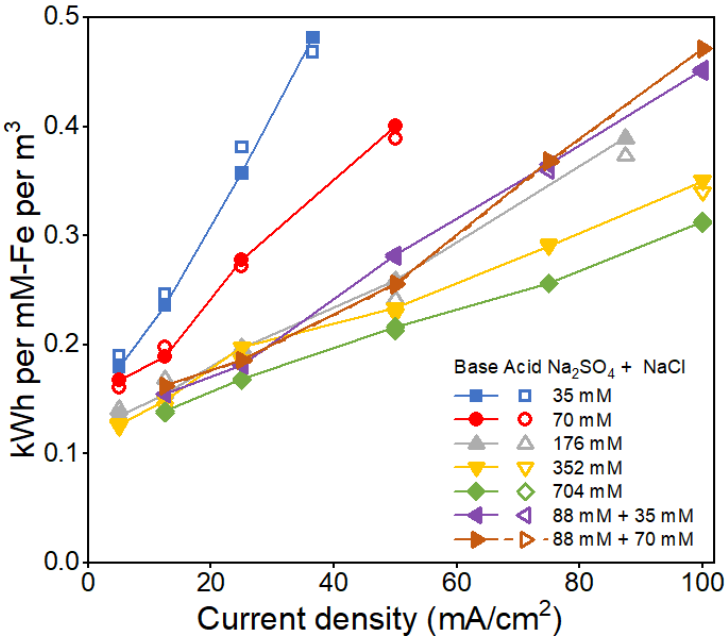

Figure 8. Electrical energy in kWh required for delivering a 1 mM Fe^{3+} dose per cubic meter of water as a function of current density.

Table 2. Costs for energy, iron and combined operational cost for the ECG process for treating 1 m^3 of FPW with 1 mM Fe^{3+}. Costs for the ECG process were increased by 10% to account for treated water recycling for acid and base production.

Operating Costs	
electrical	$0.044
iron	$0.043
total	$0.087

Conclusions

The ECG process is functionally similar to conventional electrocoagulation in that metallic iron is used to provide a ferric iron coagulant. However, in addition to lower iron costs, the ECG process overcomes several limitations of EC, especially when treating flowback and produced water. Brines generated during oil production contain suspended particles and emulsified oil that can foul EC electrodes and are usually anoxic. The ECG process eliminates electrode fouling by passing only treated water through the electrochemical cell. Anoxic waters require aeration prior to EC using iron electrodes, whereas the ECG process aerates the water at oxygen partial pressures greater than 1 atmosphere. The ECG process is also beneficial in other applications requiring high coagulant doses where a high salinity brine stream is available, such as in treatment of concentrate solutions generated during reverse osmosis production of potable water.

Supporting Information

Electrochemical cell wiring diagram, operating voltages and cell pressures versus elapsed time of operation, composition of simulated brine solution, photographs of cell cathode and cathode facing membrane and data tables for each figure.

Acknowledgements

This research was funded by the US Department of Energy and administered by the National Energy Technology Laboratory through agreement DE-FE0031854. Additional funding was provided by the Stevens Family Trust through a gift to the University of Arizona.

Disclaimer

This report was prepared as an account of work sponsored by an agency of the United States Government. Neither the United States Government nor any agency thereof, nor any of their employees, makes any warranty, express or implied, or assumes any legal liability or responsibility for the accuracy, completeness, or usefulness of any information, apparatus, product, or process disclosed, or represents that its use would not infringe privately owned rights. Reference herein to any specific commercial product, process, or service by trade name, trademark, manufacturer, or otherwise does not necessarily constitute or imply its endorsement, recommendation, or favoring by the United States Government or any agency thereof. The views and opinions of authors expressed herein do not necessarily state or reflect those of the United States Government or any agency thereof.

Graphical Abstract

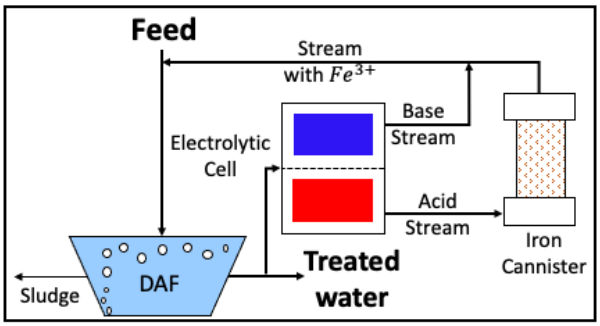

References

(1) Lowry, T.S.; Schuhen, M.D.; Lofton, O.W.; Walker, L.T.N.; Johnson, P.B.; Powers, D.W.; Bowman, D.O. Water Resource Assessment in the New Mexico Permian Basin, Sandia Report SAND2018-12018 Unlimited Release, Printed October 2018.

(2) Roland, J; Sungchung, S., The Water Stressed American West, Center for American Progress, June 26, 2019, https://www.americanprogress.org/article/oil-gas-development-creating-problem-arid-west/. accessed 2/3/2023

(3) Otton, J.K.; Mercier, T. Produced Water Brine and Stream Salinity, US Geological Survey, https://water.usgs.gov/orh/nrwww/Otten.pdf. accessed 2/3/2023

(4) Hoagland, F.M., Recycling Produced Water, presented at: Fundamentals of Produced Water Treatment in the Oil and Gas Industry, Upstream O&G Subcommittee of Industrial Wastewater Committee (IWWC), Water Environment Federation with Produced Water Society, April 25, 2019.

(5) Wilson, B.C.; Lucero, A.A., Romero, J.T.; Romero, P.J.; Water Use by Categories in New Mexico Counties and River Basins, and Irrigated Acreage in 2000, New Mexico Office of the State Engineer, Technical Report 51, February 2003.

(6) Hoagland, F.M. Introduction to Produced Water Management, presented at: Fundamentals of Produced Water Treatment in the Oil and Gas Industry Conference, Upstream O&G Subcommittee of Industrial Wastewater Committee (IWWC), Water Environment Federation with Produced Water Society, April 25, 2019.

(7) Mohammad-Pajooh, E.; Weichgrebe, D.; Cuff, G.; Tosarkani, B.M.; Rosenwinkel, K.H. On-site treatment of flowback and produced water from shale gas hydraulic fracturing: A review and economic evaluation. *Chemosphere* **2018**, 2012, 898-914.

(8) http://www.bosquesystems.com/water-treatment.html. accessed 2/3/23

(9) https://www.originclear.com/hubfs/pdf/CLEAN-FRAC-Model-60K-Data-Sheet.pdf. accessed 2/3/2023

(10) https://www.bakercorp.com/en-us/products/filtration/kaselco-systems/electrocoagulation-solutions/. accessed 2/3/2023

(11) http://www.veoliawatertech.com/news-resources/datasheets/ross-flowback-produced-water.htm. accessed 2/3/2023

(12) Freedman, D.E., Riley, S.M., Jones, Z.L., Rosenblum, J.S., Sharp, J.O., Spear, J.R. and Cath, T.Y. Biologically active filtration for fracturing flowback and produced water treatment. *Journal of Water Process Engineering* **2017,** *18*, 29-40.

(13) Chang, H., Li, T., Liu, B., Vidic, R.D., Elimelech, M. and Crittenden, J.C. Potential and implemented membrane-based technologies for the treatment and reuse of flowback and produced water from shale gas and oil plays: A review. *Desalination* **2019**, *455*, 34-57.

(14) Schulz, M.C.; Baygents, J.C.; Farrell, J. Laboratory and Pilot Testing of Electrocoagulation for removing scale-forming species from industrial process waters. *Int. J. Env. Sci. Technol.* **2009**, 6, 521-526.

(15) Gu, Z; Liao, Z.; Schulz, M.; Davis, J. R.; Baygents, J. C.; Farrell, J. Estimating dosing rates and energy consumption for electrocoagulation using iron and aluminum electrodes. *Ind. Eng. Chem. Res.* **2009**, 48, 3112-3117.

(16) Esmaeilirad, N.; Carlson, K.; Ozbek, O. Influence of softening sequence on electrocoagulation treatment of produced water. *J. Hazard. Mater.* **2015**, 283, 721-729.
(17) Aly, D.T.A. A Novel Electrocoagulation System of Produced Water Treatment, M.S. Thesis, Qatar Univeristy, January 2018.
(18) Ammar, S.H.; Akbar, A.S. Oilfield produced water treatment in internal-loop airlift reactor using electrocoagulation/flotation technique. *Chinese J. Chem. Eng*. **2018**, 26, 879-885.
(19) Lobo, F.L.; Wang, H.; Huggins, T.; Rosenblum, J.; Linden, K G., Low-energy hydraulic fracturing wastewater treatment via AC powered electrocoagulation with biochar. *J. Hazard. Mater.* **2016**, 309, 180-184.
(20) Cooper,W.J.; Roscher,N.M.; Slifker, R.A. Determining free available chlorine by DPD-colorimetric, DPD-Steadifac (colorimetric), and FACTS procedures. *Journal-American Water Works Association* **1982**, 74.7, 362-368.
(21) Tamura, H.; Goto, K., Yotsuyanagi, T.; Nagayama, M., Spectrophotometric determination of iron (II) with 1,10-phenanthroline in the presence of large amounts of iron (III). *Talanta* **1974**, 21(4), 314-318.
(22) Zendejas Rodriguez, A.; Wang, H.; Hu, L.; Zhang, Y.; Xu, P. Treatment of produced water in the Permian Basin for hydraulic fracturing: comparison of different coagulation processes and innovative filter media. *Water* **2020**, *12*, 770; doi:10.3390/w12030770
(23) Sáez, A.E.; Baygents, J.C. *Environmental transport phenomena*. CRC Press, 2014.
(24) https://www.eia.gov/totalenergy/data/monthly/pdf/sec9_11.pdf. accessed on 5/4/2023
(25) https://alliancechemical.com/product/sulfuric-acid-93/?attribute_pa_size=275-gallon&attribute_pa_packaging-type=tote&gclid=EAIaIQobChMI9JX469Xm_gIVNh-tBh2NzglVEAQYASABEgLf6PD_BwE. accessed 5/9/2023
(26) https://alliancechemical.com/product/sodium-hydroxide-50/. accessed on 5/9/2023
(27) Burke, S.P., Banwart, S.A. A geochemical model for removal of iron(II)(aq) from mine water discharges. *Appl. Geochem*. **2002**, 17, 431-443.
(28) Wehrli, B. Redox Reactions of Metal Ions at Mineral Surfaces, In: Aquatic Chemical Kinetics, W. Stumm, Ed., Wiley-Interscience, New York, 1990.
(29) Revie, R. Winston, ed. *Uhlig's corrosion handbook*. Vol. 51, John Wiley & Sons, 2011.
(30) Juchniewicz, R.; Walaszkowski, J.; Bohdanowicz, W.; Sokolski, W.; Widuchowski, A. Influence of pulsed current on platinized titanium and tantalum durability. *Corrosion Science* **1986**, 26, 55-61.

Supporting Information

Electrolytic Coagulant Generation for Treating Flowback and Produced Water for Reuse

Tenzin Phakdon[a], Jiale Xu[b], James Farrell[a*]

[a]Department of Chemical and Environmental Engineering

University of Arizona, Tucson AZ 85721

[b]Civil, Construction and Environmental Engineering

North Dakota State University, Fargo, ND 58105

*corresponding author: Department of Chemical and Environmental Engineering, University of Arizona, Tucson, AZ 85721; phone: (1) 520-940-0487; orcid.org/0000-0002-4342-7587; email: farrellj@arizona.edu

11 pages
3 figures
13 tables

Supporting Information

Electrochemical Cell Wiring Diagram

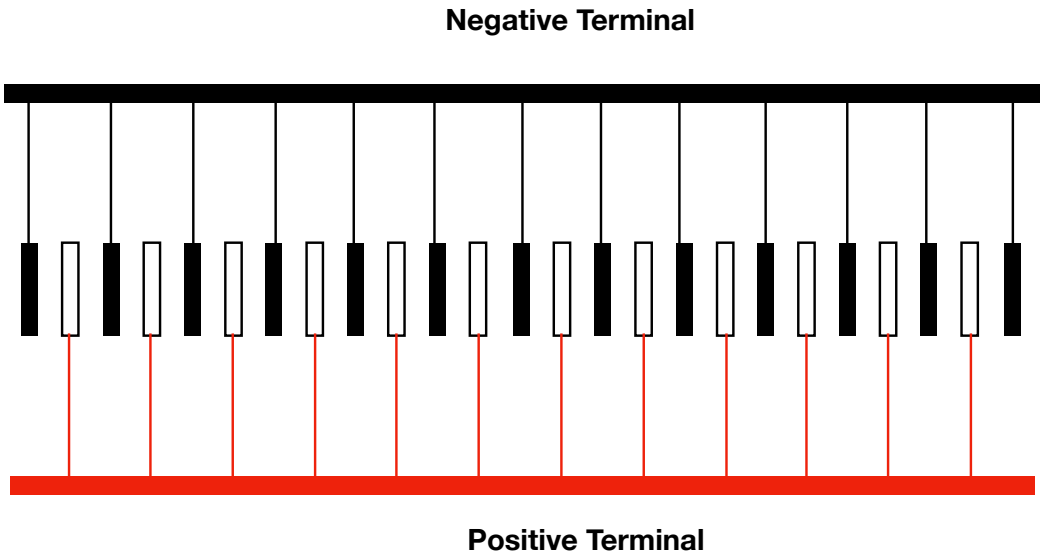

Figure S1. Electrode wiring diagram for 24 unit cells containing 12 anodes (positive) and 13 cathodes (negative) with both electrode faces active (excepting the end cathodes).

Electrode and Membrane Fouling

Figure S2a shows the operating voltages during forward and reverse polarity at 50 mA/cm^2. In forward polarity the operating voltage remained constant at 4.2 V for 3 hours before increasing to 4.3 V. Reversing the polarity decreased the cell voltage to 3.8-4.0 V. Going back to forward polarity between 4 and 5 hours elapsed, the cell voltage returned to 3.8 V and gradually increased to 4.2 V. After 5 hours elapsed, the system was put into reverse polarity for 9 hours. During this time the cell voltage increased from 3.7 to 4.5 V. Figure S2b shows the pressure required to maintain 1 liter per minute per unit cell during forward polarity. A significantly higher pressure was required for the base solution due to greater gas generation at the cathode, as indicated by the reaction stoichiometry shown in equations S1 and S2.

$$anode\ reaction \quad 2\,H_2O \rightarrow O_2 + 4\,H^+ + 4\,e^- \tag{S1}$$

$$cathode\ reaction \quad 4\,H_2O + 4\,e^- \rightarrow 2\,H_2 + 4\,OH^- \qquad \text{(S2)}$$

The stable pressure over the course of the experiment indicates the absence of cell clogging by precipitated mineral solids.

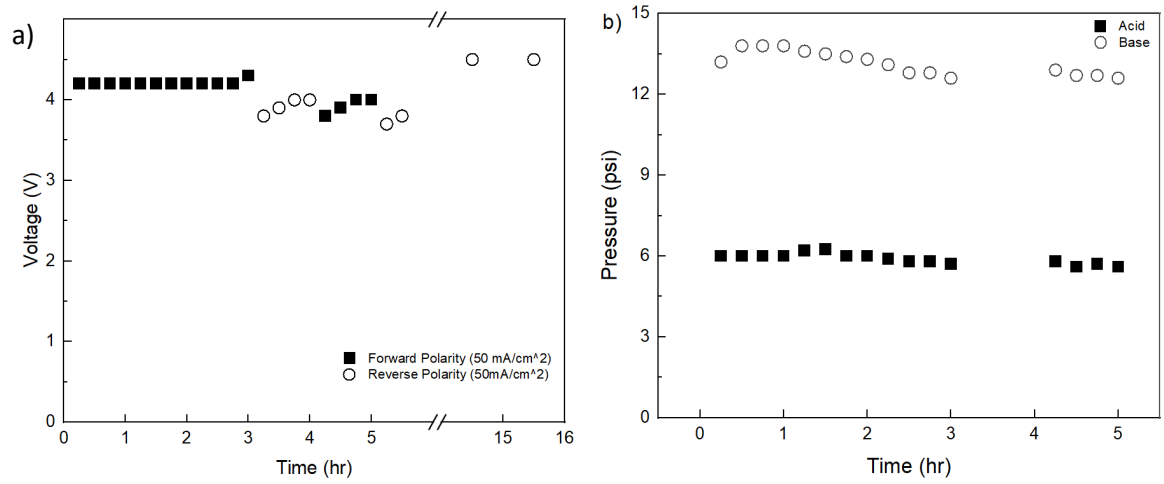

Figure S2. a) Voltage versus time of operation in forward and reverse polarity at 50 mA/cm^2. b) Influent pressure to the acid and base chambers of the electrochemical cell at a constant flow rate of 1 liter per minute per unit cell. Cell operated using feed water with composition given in Table S1.

Table S1. Composition of simulated brine solution compared to oilfied brine from Jal, New Mexico, USA (1).

Parameter	**Jal Well**	**Experiment**
pH	7.3	7.6
Ca^{2+}	4247 mg/L	4240 mg/L
Mg^{2+}	727 mg/L	730 mg/L
HCO_3^-	2867 mg/L	3050 mg/L
Na^+	42,720 mg/L	36,800 mg/L
Cl^-	65,800 mg/L	56,800 mg/L

Figure S3 shows the cathode and cathode facing membrane after operating the cell for two hours at a current density of 100 mA/cm^2.

Figure S3. Cathode and cathode facing membrane after 2 hours of operation at a current density of 100 mA/cm^2 using feed water with the composition given in Table S1. No cleaning cycle was used in this experiment.

References

(1) Zendejas Rodriguez, A.; Wang, H.; Hu, L.; Zhang, Y.; Xu, P., Treatment of produced water in the Permian Basin for hydraulic fracturing: comparison of different coagulation processes and innovative filter media, *Water* **2020**, *12*, 770; doi:10.3390/w12030770

Data for Figure 2a.

Flow Rate (L/min)	Base (mM)	Acid (mM)	Chlorine (mM)
0.05	48.5	48.8	20.0
0.25	19.2	18.6	7.0
0.5	12.1	12.0	4.3
1	6.17	6.18	2.18

Data for Figure 2b.

Flow rate (L/min)	Faradaic Efficiency Base (%)	Faradaic Efficiency Acid (%)
0.2	38.9	39.2
0.25	77.2	74.7
0.5	96.9	96.1
1	99.1	99.1

Data for Figure 2c.

Flow Rate (L/min)	HClO/Total Acid (%)
0.05	41.0
0.25	37.8
0.5	35.9
1	35.3

Data for Figure 2d.

Flow Rate (L/min)	Energy Cost Base (kWh per kmol)	Energy Cost Acid (kWh per kmol)
0.2	153.1	152.2
0.25	77.3	79.9
0.5	61.5	62.0
1	60.2	60.1

Data for Figure 3.

Current Density $\frac{mA}{cm^2}$	Base Energy Cost ($\frac{kWh}{kmol}$)						
	35 mM Na_2SO_4	70 mM Na_2SO_4	176 mM Na_2SO_4	352 mM Na_2SO_4	704 mM Na_2SO_4	88 mM Na_2SO_4 + 35 mM NaCl	88 mM Na_2SO_4 + 70 mM NaCl
5	57.5	53.6	43.2	40.7			
12.5	75.6	60.4	49.7	47.9	44.5	49.6	52.0
25	114.4	88.8	63.1	63.3	54.0	58.0	59.6
36.6	154.1			75.0	69.2	90.4	81.9
50		128.1	83.0				
75				93.1	82.0	116.8	118.0
87.5			124.7				
100				112.1	100.1	144.8	151.0

Current Density $\frac{mA}{cm^2}$	Acid Energy Cost ($\frac{kWh}{kmol}$)						
	35 mM Na_2SO_4	70 mM Na_2SO_4	176 mM Na_2SO_4	352 mM Na_2SO_4	704 mM Na_2SO_4	88 mM Na_2SO_4 + 35 mM NaCl	88 mM Na_2SO_4 + 70 mM NaCl
5.0	60.8	51.5	45.0	40.1			
12.5	78.8	63.3	53.9	45.8	44.2	49.5	51.8
25.0	121.9	87.1	63.2	59.4	53.5	57.9	59.4
36.6	149.8			73.3	68.1	89.9	81.6
50.0		124.6	77.3				
75.0				93.6	82.1	115.0	117.5
87.5			119.5				
100.0				108.8	99.7	144.2	150.8

Data for Figure 4.

Time (min)	$\frac{CH^{+}_{initial} - CH^{+}_{effluent}}{CFe}$
10	1.61
20	1.72
30	0.75
40	1.16
50	1.63
60	1.70
70	1.69
80	1.59
90	1.53
100	1.64
110	1.62
120	1.57

Data for Figure 5.

EBCT	H+ consumption percentage (%)	
(min)	88 mM Na_2SO_4	88 mM Na_2SO_4 + 35 mM NaCl
14	99	
5	62	
2.2	48	
1.4	41	
1	36	
3.5		99.98
2.3		99.97
1.8		99.97

Data for Figure 6.

Time (hr)	Forward Polarity (V)	Reverse Polarity (V)
0.5	6.9	
1	7	
1.5	7	
2	7	
3	7.1	
4	7.1	
5	7.1	
6	7.1	
6.5	7.2	
7		7.6
7.5		7.6
8		7.5
8.5		7.5
9		7.5

Data for Figure 7.

Fe Dose (mM)	pH	Turbidity (NTU)	Dissolved Fe concentration (μM)
0	6.04	92	0
1.25	5.9	1.33	10.92
1.5	5.52	2.05	9.85
1.75	5.36	1.97	11.82
2	5.28	2.7	12.18
2.25	4.85	2.03	11.82
2.5	4.74	1.77	13.79

Data for Figure 8.

Current Density $\frac{mA}{cm^2}$	Base Energy Cost $\left(\frac{kWh}{mM-Fe\ m^3}\right)$						
	35 mM Na_2SO_4	70 mM Na_2SO_4	176 mM Na_2SO_4	352 mM Na_2SO_4	704 mM Na_2SO_4	88 mM Na_2SO_4 + 35 mM NaCl	88 mM Na_2SO_4 + 70 mM NaCl
5	0.18	0.17	0.13	0.13			
12.5	0.24	0.19	0.16	0.15	0.14	0.15	0.16
25	0.36	0.28	0.20	0.20	0.17	0.18	0.19
36.6	0.48						
50		0.40	0.25946	0.23	0.22	0.28	0.26
75				0.29	0.26	0.37	0.37
87.5			0.39				
100				0.35	0.31	0.45	0.47

Current Density $\frac{mA}{cm^2}$	Acid Energy Cost $\left(\frac{kWh}{mM-Fe\ m^3}\right)$						
	35 mM Na_2SO_4	70 mM Na_2SO_4	176 mM Na_2SO_4	352 mM Na_2SO_4	704 mM Na_2SO_4	88 mM Na_2SO_4 + 35 mM NaCl	88 mM Na_2SO_4 + 70 mM NaCl
5	0.19	0.16	0.14	0.13			
12.5	0.25	0.20	0.17	0.14	0.14	0.15	0.16
25	0.38	0.27	0.20	0.19	0.17	0.18	0.19
36.6	0.47						
50		0.39	0.24	0.23	0.21	0.28	0.25
75				0.29	0.26	0.36	0.37
87.5			0.37				
100				0.34	0.31	0.45	0.47

Data for Figure S2a.

Time (hr)	Forward Polarity (V)	Reverse Polarity (V)
0.25	4.2	
0.5	4.2	
0.75	4.2	
1	4.2	
1.25	4.2	
1.5	4.2	
1.75	4.2	
2	4.2	
2.25	4.2	
2.5	4.2	
2.75	4.2	
3	4.3	
3.25		3.8
3.5		3.9
3.75		4
4		4
4.25	3.8	
4.5	3.9	
4.75	4	
5	4	
5.25		3.7
5.5		3.8
14.5		4.5
15.5		4.5

Data for Figure S2b.

Time (hr)	Acid Pressure (psi)	Base Pressure (psi)
0.25	6	13.2
0.5	6	13.8
0.75	6	13.8
1	6	13.8
1.25	6.2	13.6
1.5	6.25	13.5
1.75	6	13.4
2	6	13.3
2.25	5.9	13.1
2.5	5.8	12.8
2.75	5.8	12.8
3	5.7	12.6
4.25	5.8	12.9
4.5	5.6	12.7
4.75	5.7	12.7
5	5.6	12.6